

Synthesis, Theoretical Studies, Cytotoxicity of 2-((4-(Dimethylamino)Benzylidene)Amino)-5-Methylphenol with Potential JNK1 Inhibitory Activity

Potansiyel JNK1 İnhibe Edici Aktiviteye Sahip 2-((4-(dimetilamino)benziliden)amino)-5-metilfenol'ün Sentezi, Teorik Çalışmaları, Sitotoksitesisi

Oğuzhan KARAOSMANOĞLU ^{1*}, Halil BERBER ², Ülkü Dilek UYSAL ²

¹ Karamanoğlu Mehmetbey University, Kamil Özdağ Science Faculty, Biology Department, Karaman, Turkey
² Eskişehir Technical University, Science Faculty, Chemistry Department, Eskişehir, Turkey

ABSTRACT

Cisplatin, doxorubicin, hydroxycamptothecin, leucovorin, vincristine and 5-fluorouracil resistance of cancer cells are associated with the activities of C-Jun N-Terminal Kinase 1 (JNK1). Inhibition of the JNK1 by pharmacological agents could be a beneficial attempt for reversing the chemoresistance of various cancer cells. However, there is no FDA-approved JNK inhibitor for safe use in clinics in today's clinics. In this study, a Schiff base 2-((4-(dimethylamino)benzylidene)amino)-5-methylphenol, (7S4) has been synthesized and characterized by ¹H, ¹³C-NMR, FT-IR and elemental analysis. The stable geometry of 7S4 has been determined by DFT method with Gaussian09 program (B3LYP/6-311g++(d,p)). The Gibbs Free energies, stable tautomer forms, H-bond, Mulliken charges, dipole moment, natural bond orbital (NBO), HOMO, LUMO and band gap energy (E_{GAP}), molecular electrostatic potential (MEP) and solvent accessibility surface areas (SASA) have been calculated. Drug-likeness, anticancer and JNK1 inhibitory activities of 7S4 have been evaluated. Enol tautomer form of trans 7S4 was characterized as the most stable structure. 7S4 was observed to be a reactive compound in chemical reactions with a low E_{GAP} value. In addition, high and low electron density regions of 7S4 are responsible for the establishment of chemical bonds in biological systems. 7S4 exhibited strong druggability with the agreement on Lipinski, Ghose, Veber, Egan, and Muegge rules. Cytotoxicity tests and molecular docking revealed that 7S4 poses a potential JNK1 inhibitor activity.

Keywords: Schiff bases, DFT method, JNK1 inhibitors, antitumor agents, druglikeness, molecular docking

Alınış / Received: 06.06.2023 Kabul / Accepted: 03.08.2023 Online Yayınlanma / Published Online: 15.08.2023



Ö Z

Kanser hücrelerinin sisplatin, doksorubisin, hidrokamptotesin, lökovorin, vinkristin ve 5-fluorourasil direnci, C-Jun N-Terminal Kinaz 1 (JNK1) aktiviteleri ile ilişkilidir. JNK1'in farmakolojik ajanlar tarafından inhibisyonu, çeşitli kanser hücrelerinin kemodirencini tersine çevirmek için yararlı bir yaklaşım olabilir. Ancak günümüz kliniklerinde güvenli kullanım için FDA onaylı bir JNK inhibitörü bulunmamaktadır. Bu çalışmada, bir Schiff bazı 2-((4-(dimetilamino)benziliden)amino)-5-metilfenol, (7S4) sentezlenmiş ve ¹H, ¹³C-NMR, FT-IR ve element analizi ile karakterize edilmiştir. 7S4'ün kararlı geometrisi Gaussian09 programı (B3LYP/6-311g++(d,p)) ile DFT yöntemi ile belirlenmiştir. Gibbs Serbest enerjileri, kararlı tautomer formları, H-bağı, Mulliken yükleri, dipol momenti, doğal bağ orbital (NBO), HOMO, LUMO ve bant boşluk enerjisi (EGAP), moleküler elektrostatik potansiyel (MEP) ve çözücü erişilebilirlik yüzey alanları (SASA) hesaplanmıştır. 7S4'ün ilaca benzerliği, antikanser ve JNK1 inhibitör aktiviteleri değerlendirilmiştir. Trans 7S4'ün enol tautomer formu en kararlı yapı olarak nitelendirildi. 7S4'ün düşük EGAP değeri ile kimyasal reaksiyonlarda reaktif bir bileşik olduğu gözlemlendi. Ayrıca 7S4'ün yüksek ve düşük elektron yoğunluklu bölgeleri biyolojik sistemlerde kimyasal bağların kurulmasından sorumludur. 7S4, Lipinski, Ghose, Veber, Egan ve Muegge kurallarına ilişkin anlaşma ile güçlü uyandırulabilirlik sergiledi. Sitotoksikite testleri ve moleküler kenetlenme, 7S4'ün potansiyel bir JNK1 inhibitör aktivitesi oluşturduğunu ortaya çıkardı.

Anahtar Kelimeler: Schiff bazları, DFT yöntemi, JNK1 inhibitörleri, antitümör ajanlar, ilaca benzerlik, moleküler kenetlenme



1. Introduction

Cancer is at least the second substantial reason of decease in advance the age of 70 years in 112 of 183 countries [1]. Chemotherapy is a standard method of cancer treatment that relies on cytotoxic drugs for the destruction or inhibition of the growth and metastasis of cancer cells. There has been a considerable effort to discover anticancer agents for cancer chemotherapy [2–6]. However, cancer chemotherapy often adversely affected from the chemoresistance which is the skill of tumor cells to adopt the presence of cytotoxic drugs. Various factors including personal variations in medication susceptibility, location of cancer, aggressivity of tumor, and modifications in intracellular molecules conduce the chemoresistance of cancer cells [7]. New cytotoxic drugs which are useful for overcoming chemoresistance hold significant value.

C-Jun N-Terminal Kinase 1 (JNK1) is a constituent of stress-activated protein kinases (SAPKs) that are primarily switched on in reply to cellular pressure [8]. JNK1 is involved in 5-fluorouracil and leucovorin resistance of pancreatic ductal adenocarcinoma patients [9]; cisplatin resistance of hepatocellular carcinoma and ovarian cancer cells [10,11]; doxorubicin resistance of breast cancer, chronic myelogenous leukemia, hepatocellular carcinoma, small cell lung cancer, and stomach cancer cells [12–15], vincristine resistance of epidermoid carcinoma cells [15]; hydroxycamptothecin resistance of colon cancer cells [16]; and oxaliplatin resistance of colon cancer cells [17]. Therefore, restriction of the kinase function of JNK1 by pharmacological agents could be a beneficial attempt for reversing the chemoresistance of various tumor cells. Developing efficient and specified JNK inhibitors is a quite vibrant field in distinct laboratories in the globe. In the past decade, many JNK inhibitors such as SP600125, AS601245, JNK-IN-8 were discovered [18]. However, to the best of our knowledge, there is no FDA-approved JNK1 inhibitor for safe use in clinics (<https://www.ppu.mrc.ac.uk/sites/default/files/2021-04/small-molecule-inhibitors.pdf>). There are many successful kinase inhibitors, such as imatinib, nilotinib for different kinase enzymes like ALK, B-Raf, BCR-Abl, EGFR, and VEGFR [19]. So, it is possible to assume that effective and safe small molecules can be developed to inhibit JNK1.

Schiff bases, which are small molecules, and their complexes have certain properties such as chemo sensor [20,21], catalytic [22], optical switching devices [23], solvato chromic [24,25], fluorescent material [24], and liquid crystal [26]. Compounds derived from aromatic ortho hydroxy Schiff bases are of particular interest due to their nonlinear optical properties and abilities for polymerization and metal bond formation. Moreover, various activity studies such as antifungal, antimicrobial, antimalarial, trypanocidal, antiproliferative, anti-inflammatory, antipyretic, herbicide and antitumor activity such compounds are available in the literature [20,21,33,34,22,26–32].

In this study, first of all, the synthesis and characterization of the new 2-((4-(dimethylamino)benzylidene)amino)-5-methylphenol compound (7S4) was performed. The stable structure of the compound and possible tautomer stabilities was then determined theoretically. The utility of 7S4 as an anticancer agent was evaluated in five different cancer and two control cell lines. Moreover, pharmacokinetics, druglikeness and molecular docking analysis were performed comparatively between 7S4 and previously reported JNK inhibitors that are SP600125 [35], and a Pyrrolopyrimidine [36]. The demonstration of the binding activity of the Pyrrolopyrimidine to the JNK1 by an eminent study [36] provided the possibility to compare the JNK1 inhibitory activity of 7S4, SP600125 and the Pyrrolopyrimidine. SP600125 is a bilateral ATP-competitive inhibitor of JNK1. Some of in vitro and in vivo studies proved the JNK1 inhibitor activity of SP600125 [37–39]. However, toxicity induced by SP600125 could be the major problem for the clinical utility of this small molecule [18].

2. Material and Method

Chemistry

General

All solvents and organic compounds used in the synthesis are of spectroscopic purity and were obtained from Sigma-Aldrich. Synthesis reaction of the molecule 7S4 was given in Figure 1. Spectroscopic analysis of the compound; ^1H and ^{13}C NMR spectra were performed by Agilent 400 MHz NMR Magnet Spectrometer in deuterium dimethyl sulfoxide (DMSO- d_6), FT-IR spectra were performed with KBr pellets by Perkin Elmer Spectrum 100 FT-IR Spectrometer and elemental analysis was performed on LECO-932 CHNS-O Elemental Analyzer. The original spectra (NMR and IR) of the synthesized compound 7S4 are given in Supplementary materials_experimental1.

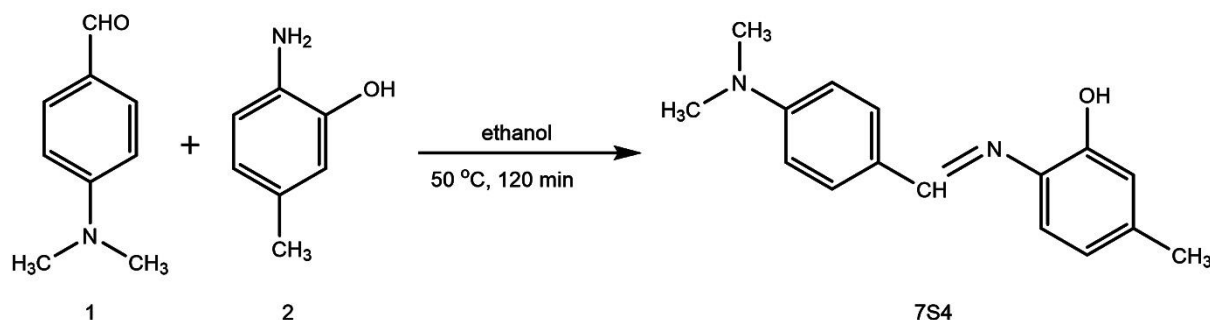


Figure 1: Synthesis reaction of 2-((4-(dimethylamino)benzylidene)amino)-5-methylphenol (7S4).

General Procedure for the Synthesis of 7S4

0.01 mole of 4-(dimethylamino)benzaldehyde (1) and 0.01 mole of 2-amino-5-methylphenol (2) compounds were dissolved in 10 mL of ethyl alcohol in separate containers by slightly heating. 2-amino-5-methylphenol solution was added to the 4-(dimethylamino)benzaldehyde solution with slow stirring. The product started to precipitate within the first 30 minutes and the mixing process was continued for another 90 minutes. The precipitated product was filtered off, then it was recrystallized in ethanol and dried first in the open air and then in a desiccator. The structure of the 7S4 was elucidated by spectroscopic techniques. 2-((4-(dimethylamino)benzylidene)amino)-5-methylphenol (7S4): FT-IR (KBr,

disk, ν cm⁻¹), 3436 (O-H), 3361, 3079, 3039 and 3002 (C-H, aromatic), 2915, 2893, 2860 and 2818 (C-H, aliphatic), 1611 (C=N), 1526 and 1499 (C=C, aromatic), 1228 (C-O, aromatic). ¹H NMR (400 MHz, dmso) δ 8.60 (s, 1H), 8.50 (s, 1H), 7.82 (d, J = 8.4 Hz, 2H), 7.07 (d, J = 8.0 Hz, 1H), 6.77 (d, J = 8.4 Hz, 2H), 6.68 (s, 1H), 6.61 (d, J = 8.0 Hz, 1H), 3.01 (s, 6H), 2.23 (s, 3H). ¹³C NMR (101 MHz, dmso) δ 157.81 (s), 152.57 (s), 151.41 (s), 136.16 (s), 136.12 (s), 130.77 (s), 124.68 (s), 120.48 (s), 118.22 (s), 116.45 (s), 111.77 (s), 40.19 (s), 21.24 (s). Elemental analysis, C₁₆H₁₈N₂O, Calculated (Found), %: C, 75.56 (75.00); H, 7,13 (7,311); N, 11.01 (11.12).

Theoretical Calculation Procedure

Theoretical calculations were made by Gaussian09 [40] [34] and GaussView 5.0.9 [41] programs using the DFT/B3LYP/6-311++G(d,p) level of theory. Before Gaussian calculation; CS ChemBioDraw Ultra 16.0.1.4 for Microsoft Windows [42] and MarvinSketch 19.27.0 [43] programs were used as preliminary experiments to identify possible stable molecular structures of the compound (7S4). Calculations were made in vacuum and certain solvent phases [acetone (ACT), acetonitrile (ACCN), chloroform (CHCl₃), dichloromethane (DCM), N,N-dimethyl formamide (DMF), dimethyl sulfoxide (DMSO), ethyl alcohol (ETOH), methyl alcohol (METOH) and vacuum (V)] using the DFT/B3LYP/6-311++G(d,p) level of theory and CPCM model.

Biology

Cell culture

Five cancer and two cells including A549, Caco-2, HCT-116, Huh7, MCF-7, 3T3-L1, hTERT-HPNE were used in this study. Detailed explanations for the source and cultivation of these cell lines can be found from our previous publication [4].

Cytotoxicity

Cytotoxicity of 7S4 was assessed by neutral red uptake (NRU) assay as was described previously [4]. In brief, 10000 cells were plated to 96-well culture plate (Thermo Scientific, Germany), next incubated for an overnight at 37 °C in 5% CO₂, then 30, 15, 7.5, 3.25, 1.6, 0.8 and 0.4 μ g/mL of 7S4 were administered to cells. After the 72h incubation medium was poored, 200 μ l of 50 μ g/mL neutral red dye medium was applied to each well and cells were incubated for an extra 3h. Further, the neutral red medium was discarded and wells were rinsed by 200 μ l phosphate buffer saline (PBS), then dye was extracted with the application of 200 μ L acidic ethanol solution comprising of acetic acid-water-ethanol (1:49:50:v:v:v). The plates were retained for 15 min at room temperature for firm extraction of the dye on an orbital-rocking shaker GFL 3012 (Gesellschaft für Labortechnik mbH, Burgwedel, Germany). Absorbance was quantified by an ELx 808 Ultra Microplate Reader (BioTek, Winooski, Vermont, USA) decorated with a 540 nm filter. Cells applied with 0.1% dimethylsulfoxide (DMSO) were used as solvent control for assessing the viability. The IC₅₀ quantities were estimated as the concentrations of test compounds that were necessary to halve the number of cells and assessed by a calibration curve as previously mentioned [44]. In the whole wells DMSO concentration was not higher than 0.1%.

In Silico Pharmacokinetics and Druglikeness

SwissADME [45] was utilized for the comparative analysis of absorption, distribution, metabolism, excretion (ADME) and druglikeness of 7S4, SP600125 and the Pyrrolopyrimidine. Chemical structures of SP600125 and the Pyrrolopyrimidine are presented in Figure 2.

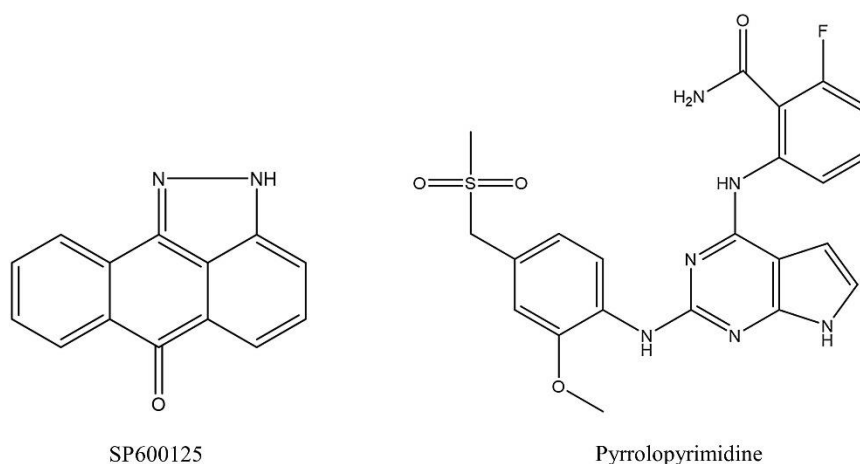


Figure 2: Chemical structures of reference compounds, SP600125 and the Pyrrolopyrimidine.

In Silico Molecular Docking

Protein Data Bank at the Research Collaboration for Structural Bioinformatics (RCSB) website [www.rcsb.org] (PDB: 3ELJ) was used for obtaining the X-ray crystal structure of JNK1 co-crystallized with the Pyrrolopyrimidine [36]. AutoDockTools-1.5.6 [46] was used for the definition of docking sites, rotatable bonds and the addition of polar hydrogen atoms. Vina forcefield was used for generating affinity maps. A selective JNK1 inhibitor, SP600125 [35] and native ligand of 3ELJ, the Pyrrolopyrimidine [36] were used as positive controls. While JNK1 was regarded as rigid, the ligands were regarded as flexible molecules in this molecular docking procedure. The binding affinity of 7S4, SP600125 and the Pyrrolopyrimidine to the JNK1 was calculated by AutoDock Vina [47]. The 3D structure of the JNK1-7S4, SP600125 and the Pyrrolopyrimidine interaction was visualized and documented by using PyMOL [48].

3. Results

The compound 7S4, commercially purchased compounds of 4-(dimethylamino)benzaldehyde (1) and 2-amino-5-methylphenol (2), were synthesized according to the procedure outlined in experimental section using ethyl alcohol solvent. The synthesis reaction of 7S4 is shown in Figure 1. The synthesis took place at approximately 50 °C and a total of 120 minutes. After the purity of the 7S4 was proved by thin layer chromatography (TLC) technique, it was characterized by ¹H, ¹³C-NMR, FT-IR and elemental analysis. In experimental and theoretical calculations; this compound, characterized by its purity and structure, was used.

Theoretical Calculations

Identification of the Stable Structure for the Compound (7S4)

In order to identify the stable structure of the molecule (7S4), different cis and trans structures of it were drawn by the Chem Draw program. Firstly, the energy of each cis and trans structure was calculated by minimizing them with MM2 in Chem3D. Then, the second calculation was performed by conformation calculation with MarvinSketch 19.27.0 program to determine the stable structure of the 7S4. Each structure determined by the MarvinSketch program was minimized again with MM2 in Chem3D and their energies were calculated. It is determined that the most stable structure (the lowest energy structure of the compound) for 7S4 was determined by the above two methods (7S4_M7_7). Different possible stable structures were investigated by scanning calculation of the most stable structure of the 7S4 (7S4_M7_7) in Chem3D program and by using dihedral angles of imine (CH=N) and hydroxyl (O-H) groups. The possible tautomer form was drawn by using the determined most stable trans structure of the compound (7S4_M7_7). The drawn enol and keto tautomer forms were named as 7S4_M7_7_E and 7S4_M7_7_K, respectively (Figure 3).

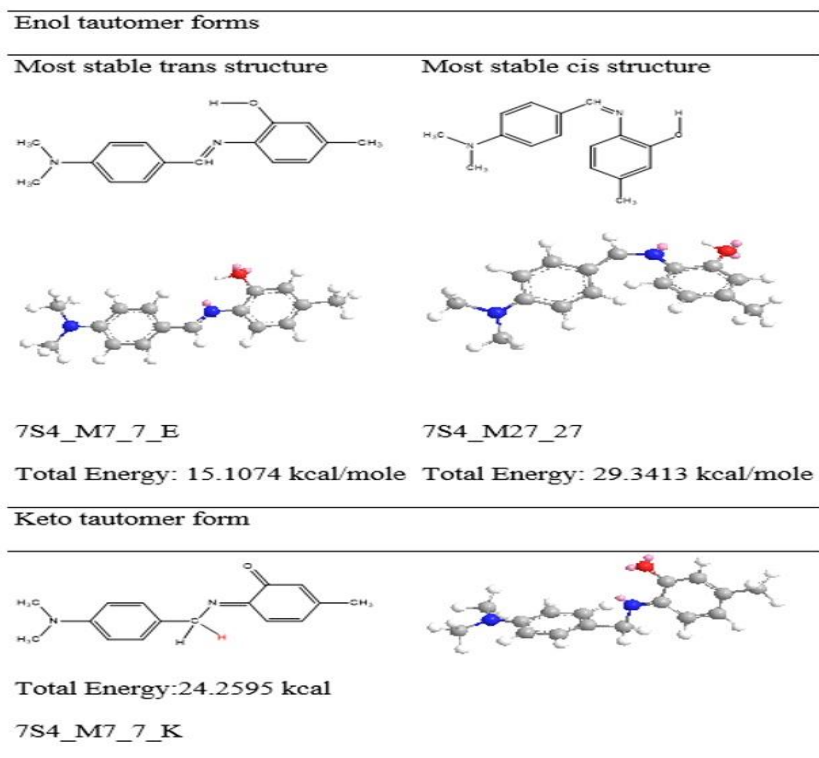
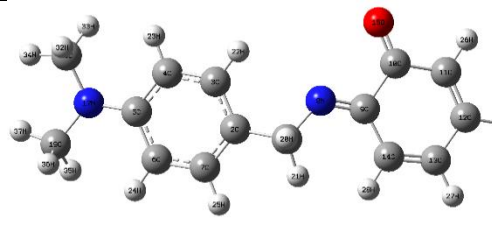
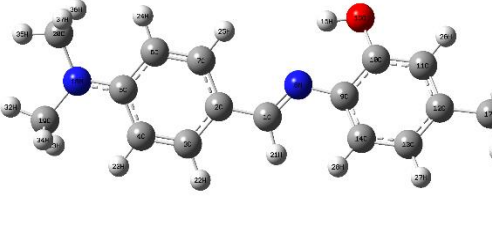


Figure 3: Shapes and minimized energies of the most stable trans and cis structures for 7S4 (E, enol form; K, possible) tautomer form.

Table 1: The bond angles, energies and shapes of the calculated most stable conformations of the 7S4 (using B3LYP method and 6-311++g(d,p) basis set).

Molecule	Dihedral angle	Energy (kcal/mole)	Conformation
1_7S4_M7_7_K_opt	2C-1C-8N-9C	138	
	3C-2C-1C-8N	41	
	15O-10C-9C-8N	0.3	
2_7S4_M7_7_E_opt	9C-10C-15O-16H	0.002	
	3C-2C-1C-8N	-0.014	
	2C-1C-8N-9C	180	
3_7S4_M7_7_E_scan150	9C-10C-15O-16H	0.004	
	3C-2C-1C-8N	-4	
	2C-1C-8N-9C	178	

4_7S4_M7_7_K_scan8 N	2C-1C-8N-9c	-139	-505412.6	
	3C-2C-1C-8N	-38		
	15O-10C-9C-8N	-0.2		
5_7S4_M7_7_E_scan8 N	9C-10C-15O-16H	3	-505446.9	
	3C-2C-1C-8N	-180		
	2C-1C-8N-9C	177		

Optimization Calculations

First of all, the optimization calculation of the 7S4_M7_7_E and 7S4_M7_7_K conformations was performed using the B3LYP method and the 6-311++g(d,p) basis set. We preferred this method and the basis set since these are the most used method and basis set in the general calculations of this molecule and similar molecules [4, 23-25]. In addition, the scan calculation of the 7S4_M7_7_E form with 9C-10C-15O-16H atoms (7S4_M7_7_E_scan15O) and 3C-2C-1C-8N (7S4_M7_7_E_scan8N) atoms were done by the B3LYP method with 6-311++g(d,p) basis set. The scan calculation of 7S4_M7_7_K form with 2C-1C-8N-9C (7S4_M7_7_K_scan8N) atoms was done by the same method and basis set. The bond angles, energies and shapes of the most stable conformations determined by this calculation are given in Table 1 (Supplementary materials1).

From the scan calculation of the enol form 7S4_M7_7_E with the angle 9C-10C-15O-16H, it was determined that the most stable conformation was 3_7S4_M7_7_E_scan15O with an energy of -505446.950 kcal/mole. This conformation was used for other enol form calculations (Supplementary materials1). From the scan calculation of the keto form 7S4_M7_7_K with the angle of 2C-1C-8N-9C, the most stable conformation was the 1_7S4_M7_7_K_opt conformation with an energy of -505412.646 kcal/mole. The conformation was used for other keto form calculations (Supplementary materials1).

Tautomer

Knowledge about the probability and ratio of the tautomer form of the molecule is important in terms of reactions, spectroscopic analyses, biological and pharmacological properties. Calculation results of 3_7S4_M7_7_E_scan15O molecule and its possible tautomer form in vacuum and solvent phase are shown in Table 2.

Table 2: SETFE energies and K_T values of the enol and keto tautomer forms of the studied molecule.

Molecule				Tautomer
31_7S4_M7_7_E_scan15O_freq		11_7S4_M7_7_K_freq		E \rightleftharpoons K
Solvent	SETFE* (kcal/mole)	Solvent	SETFE* (kcal/mole)	K_T^{**} (kcal/mole)
ACT	-505290.749	ACT	-505259.665	31.084
ACCN	-505290.928	ACCN	-505259.965	30.963
CHCl3	-505291.234	CHCl3	-505257.446	33.788
DCM	-505290.217	DCM	-505258.778	31.438
DMF	-505291.832	DMF	-505258.023	33.810
DMSO	-505290.985	DMSO	-505260.062	30.924
ETOH	-505290.822	ETOH	-505259.787	31.035
METOH	-505290.905	METOH	-505259.927	30.978

* SETFE: Sum of electronic and thermal free energies

**The K_T tautomer shows the tautomer equilibrium values between the enol form (31_7S4_M7_7_E_scan15O_freq) and the keto form (11_7S4_M7_7_K_freq). $K_T = SETFE_K - SETFE_E$ (negative value indicates that form E is more stable)

Since the K_T tautomer has positive values in vacuum and in all solvents (approximately 30-33 kcal/mole), it seems that the enol tautomer forms are more stable and the equilibrium is towards the enol form. This means that the probability of formation of the K_T tautomer form in the reaction medium is very unlikely. The most stable enol form (31_7S4_M7_7_E_scan15O_freq) of the compound determined by tautomer calculation was used in all other calculations.

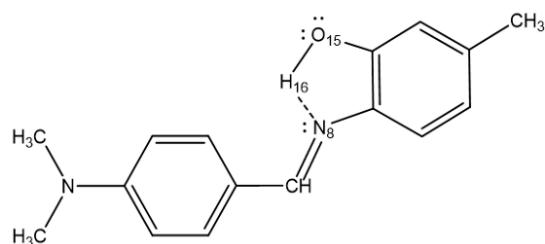
Intramolecular H-bond

The B3LYP method and the Natural Atomic Orbital and Natural Bond Orbital (NBO) Analysis calculations on the 6-311g++(d,p) basis set were calculated in vacuum by Gaussian NBO Version 3.1. The calculated H-bond values are given in Figure 4.

The intramolecular H-bond affects the stability of the molecule. In the tautomer equilibrium (K_T) of the calculated enol and keto forms; the contribution of the H-bond is also inevitable for the balance to favor the enol form. Intramolecular H-bonding is observed only in the enol form and not in the keto form. The fact that the calculated intramolecular H-bond was 2.033 Å caused the enol form to be more stable, and due to this situation, the high K_T values in the tautomer equilibrium (30-33 kcal/mole) resulted in the equilibrium being towards the enol form.

Dipole Moment

The dipole moment value gives information about the charge distribution in the molecule. In addition, a high dipole moment means that the charge distribution is dense in different atoms groups or regions in the molecule, and low means that it is less. The dipole moment also helps us to understand solvent-solute interaction. Dipole moment values in frequency calculation in vacuum by B3LYP method and on 6-311g++(d,p) basis set are given in Table 3.



31_7S4_M7_7_E_scan150_freq

Bond length (Å)

H16.....N8

2.033

Figure 4: Intramolecular H-bond.

It was observed that the dipole moment values were high (approximately 5-7 Debye) in the form 31_7S4_M7_7_E_scan150_freq. Since the dipole moment of the form of 31_7S4_M7_7_E_scan150_freq is high, it is understood that the charge is polarized in certain atoms, groups and regions (see section molecular electrostatic potential (MEP)). The higher electronegativity of nitrogen and oxygen compared to hydrogen and carbon causes the change in the charge distribution of the changing functional groups in the molecular structure, and therefore the dipole moment to be higher. High dipole moment value means that the compound dissolves more easily in polar and protic solvents.

Table 3: Dipole moment values.

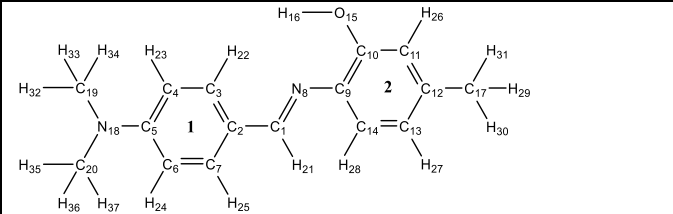
Molecule	
31_7S4_M7_7_E_scan150_freq	
Solvent	Dipole (Debye)
ACT	7.813
ACCN	7.869
CHCl3	7.399
DCM	7.646
DMF	7.506
DMSO	7.888
ETOH	7.836
METOH	7.862
V	5.945

Natural Bond Orbital (NBO)

Electron-rich and electron-deficient centers in the molecule are determined by calculating the atomic charges. Knowing the electron-rich or electron-deficient atoms and centers helps us to know the center where electrophiles or nucleophiles will attack in reactions and to understand the reaction mechanism. Another advantage of knowing the atomic charges is that it allows us to predict the solvent-solute interaction, intramolecular or intermolecular H-bonding. Also, basic and acidic centers can be estimated. If the molecule has a biologically active property, it can be predicted from which atom or functional group the may be active. If the molecule is used as a ligand in complex reactions, it can be understood with which atoms the coordinate covalent bond will be formed. NBO calculation for stable enol form was done with B3LYP method and 6-311g++(d,p) basis set in vacuum by Gaussian NBO Version 3.1 (Table 4).

According to the NBO calculation results, it is seen that the aromatic ring (1) with C2-C7 carbon atoms contains more electron-rich atoms (with lower negative values) than the atomic charges in the aromatic ring (2) with C9-C14 carbon atoms (Table 4). The higher charges of the C2-C7 carbon atoms are due to the strong mesomeric electron repulsion to the ring with the contribution of the N18 (N(CH₃)₂) atom and the methyl group attached to this atom. In the aromatic ring with C9-C14 carbon atoms, there is weak mesomeric electron repulsion of the O15 atom and the C17 methyl group attached to the ring (Table 4). In the compound, they are hetero atoms with the highest electron charge and their electron charges are O15: -0.681, N8: -0.514 and N18: -0.477, respectively. The polarity and activity of the molecule are due to these heteroatoms. Of all the hydrogens, the hydrogen with the fewest electrons, that is, the most electron-deprived (with the higher positive value), is hydrogen H16: 0.489. Since hydrogens with a higher positive value are usually acidic hydrogens, it can be said that hydrogen H16 is acidic hydrogen. The theoretical pKa calculation was calculated for H16 as pKa=8.582 with the PM6 method by MOPAC2016 package program.

Table 4: Natural Bond Orbital (NBO).



Atom No	Natural Charge*	Atom No	Natural Charge*
C1	0.152	C20	-0.351
C2	-0.166	H21	0.149
C3	-0.134	H22	0.217
C4	-0.257	H23	0.208
C5	0.212	H24	0.208
C6	-0.276	H25	0.204
C7	-0.131	H26	0.211
N8	-0.514	H27	0.199
C9	0.061	H28	0.201
C10	0.337	H29	0.211
C11	-0.257	H30	0.204
C12	-0.016	H31	0.208
C13	-0.230	H32	0.199
C14	-0.202	H33	0.186
O15	-0.681	H34	0.195
H16	0.489	H35	0.199
C17	-0.587	H36	0.186
N18	-0.477	H37	0.194
C19	-0.351		

* Negative charge values mean electron rich and positive charge values mean electron weak.

HOMO, LUMO and Band Gap Energy (E_{GAP})

The HOMO and LUMO energies of the molecule and the difference between these two energies (band gap energy, E_{GAP}) help us to understand the chemical behavior, optical, electronic, conductivity, etc. properties of the molecule. The HOMO, LUMO and E_{GAP} energy values and shapes determined by the calculation made with the DFT TD-SCF B3LYP method and the 6-311g++(d,p) basis set are given in Figure 5. From the E_{HOMO} and E_{LUMO} calculations, it was determined that the electrons were distributed throughout the molecule and the ΔE_{GAP} energy (2.366 eV) was not very high.

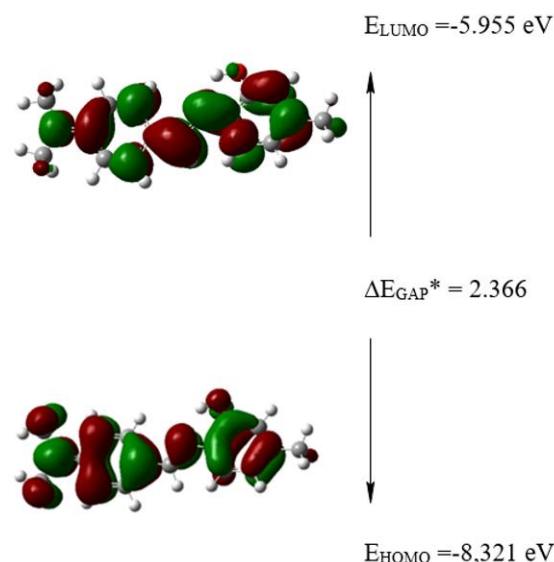


Figure 5: E_{HOMO} , E_{LUMO} and E_{GAP} values of the studied molecule.

Molecular Electrostatic Potential (MEP)

Molecular electrostatic potential energy maps allow us to see the charge distributions of molecules in three dimensions and to visually see the charged regions of the molecule. The red color represents the region with the most electrons (electron rich) and the blue area represents the region with the least electrons (electron weak). The MEP shape of the molecule determined by the calculation made with the DFT B3LYP method and the 6-311g++(d,p) basis set is given in Figure 6. The electron-rich center of the molecule is the aromatic ring containing OH and the other aromatic ring is less electron-rich (Figure 6). It is seen that the methyl groups attached to the amine are the electron weakest center, and the hydrogens in the molecule are also electron weak.

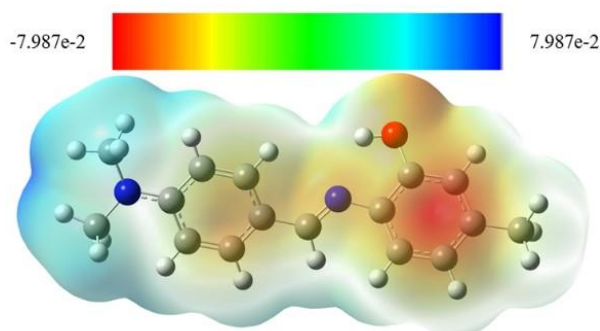


Figure 6: Molecular electrostatic potential (MEP) shape of the molecule.

Solvent Accessible Surface Area (SASA)

SASA (Solvent accessible surface area) is an image that helps us see how a molecule dissolved or to be dissolved in the solvent interacts with the solvent molecule. The SASA shape determined by the calculation made with the DFT B3LYP method and the 6-311g++(d,p) basis set is given in Figure 7. In the Figure 7, blue and red atoms represent polar centers, and gray colors represent nonpolar centers. It means that polar and polar protic solvents will be activated with blue and red colored atoms and nonpolar solvents will be activated with gray colored atoms.

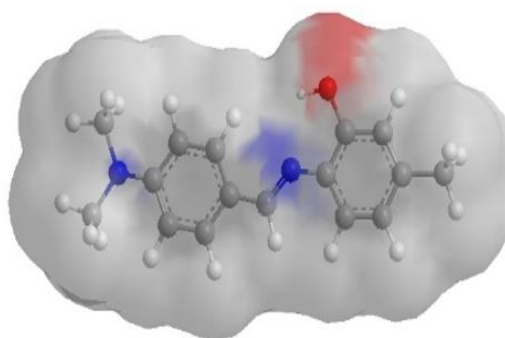


Figure 7: The SASA shape of the molecule.

Cytotoxicity

By using the NRU assay the cytotoxicity of 7S4 was screened on five cancer cells including A549, Caco-2, HCT-116, Huh-7, MCF-7; and two normal cells including hTERT-HPNE and 3T3-L1. The IC₅₀ values that were the 7S4 concentration to halve the cell number and the selectivity indexes (SIA, SIB) that were the division of 7S4 concentration to halve the hTERT-HPNE cells and the 7S4 concentration to halve the 3T3-L1 cells were by the 7S4 concentration to halve the cancer cells, were calculated and presented in Table 5. It was observed that the 7S4 concentration to halve the cell number was higher than 11.85 µg/mL and increased among the cell lines with the order of 3T3-L1, Huh-7, MCF-7, HCT-116, A549, hTERT-HPNE, and Caco-2. Caco-2 was the most resistant and 3T3-L1 was the most sensitive cell line for the 7S4 induced toxicity. When the SIA values were compared it was observed that Huh-7 cells were 1.9-fold MCF-7 cells were 1.67-fold sensitive to the 7S4 induced cytotoxicity than the normal hTERT-HPNE cells. This result implies a role for the selective toxicity for 7S4 to the hepatocellular carcinoma and breast cancer cells. However, this idea weakens when the S2 values that were 0.82 and 0.71 are considered. Therefore, it was concluded that 7S4 was moderately toxic to both cancer and normal cells.

Table 5: IC₅₀ values* (µg/mL) and selectivity indexes** (SIA and SIB) of 7S4 on cancer and normal cell lines. Results from three different biological replicates were exhibited as mean ± SD.

	A549	Caco-2	HCT-116	Huh-7	MCF-7	hTERT-HPNE	3T3-L1
IC₅₀ of 7S4	27.61±3.37 (SIA 1; SIB 0.42)	>30	27.41±3.66 (SIA 1; SIB 0.43)	14.46±0.35 (SIA 1.9; SIB 0.82)	16.57±3.29 (SIA 1.67; SIB 0.71)	27.65±1.70	11.85±0.61

IC₅₀*: half inhibitory concentration; NRU: neutral red uptake; SD: standard deviation. **The selectivity indexes were calculated by the division of IC₅₀ values of hTERT-HPNE (for SIA) and 3T3-L1 (for SIB) by the cancer cell lines.

Pharmacokinetics and druglikeness

By using the SwissADME computational tool, the pharmacokinetic characteristics and druglikeness of test molecules can be predicted with an accuracy of 71% to 89% [35]. Thus, pharmacokinetic characteristics and druglikeness of 7S4, SP600125 and the Pyrrolopyrimidine were compared from SwissADME and presented in Table 6. It was observed that SP600125 and 7S4 shared common peculiarities in terms of druglikeness scores and pharmacokinetic characteristics such as gastrointestinal absorption, blood-brain barrier access, CYP450 inhibitory activities that could be better than the Pyrrolopyrimidine. Moreover, since 7S4 was predicted to be more soluble than SP600125 it was suggested that 7S4 has an advantage for being used as a pharmacological agent for inhibiting JNK1 activity.

Table 6: Comparative analysis of absorption, distribution, metabolism, and excretion (ADME) between 7S4, SP600125 and the Pyrrolopyrimidine.

	Pecularity	7S4	SP600125	Pyrrolopyrimidine
Physicochemical Properties	Formula	C ₁₆ H ₂₀ N ₂ O	C ₁₄ H ₈ N ₂ O	C ₂₉ H ₂₇ F ₂ N ₈ O ₅ S
	Molecular weight	256.34 g/mole	220.23 g/mole	637.64 g/mole
	Num. heavy atoms	19	17	45
	Num. arom. heavy atoms	6	14	6
	Fraction Csp3	0.31	0.00	0.59
	Num. rotatable bonds	3	0	6
	Num. H-bond acceptors	3	3	12
	Num. H-bond donors	1	1	5
	Molar Refractivity	80.93	74.31	169.49
	Topological molar surface area	35.83 Å ²	44.95 Å ²	211.10 Å ²
Lipophilicity	Log Po/w (iLOGP)	3.06	2.39	0.00
	Log Po/w (XLOGP3)	2.80	3.92	-2.12
	Log Po/w (WLOGP)	3.08	3.67	-1.02
	Log Po/w (MLOGP)	2.18	2.52	1.38
	Log Po/w (SILICOS-IT)	2.37	4.30	1.16
	Consensus Log Po/w	2.70	3.36	-0.12
Water Solubility	Log S (ESOL)	-3.23	-4.28	-2.16
	Solubility	1.51e-01 mg/mL ; 5.90e-04 mole/L	1.14e-02 mg/mL ; 5.20e-05 mole/L	4.41e+00 mg/mL ; 6.91e-03 mole/L
	Class	Soluble	Moderately soluble	Soluble
	Log S (Ali)	-3.21	-4.56	-1.78
	Solubility	1.58e-01 mg/mL ; 6.18e-04 mole/L	6.02e-03 mg/mL ; 2.74e-05 mole/L	1.05e+01 mg/mL ; 1.64e-02 mole/L
	Class	Soluble	Moderately soluble	Very soluble
	Log S (SILICOS-IT)	-2.69	-5.27	-5.69
	Solubility	5.27e-01 mg/mL ; 2.06e-03 mole/L	1.18e-03 mg/mL ; 5.37e-06 mole/L	1.31e-03 mg/mL ; 2.05e-06 mole/L
	Class	Soluble	Moderately soluble	Moderately soluble
	Pharmacokinetics	GI absorption	High	High
BBB permeant		Yes	Yes	No
P-gp substrate		No	No	Yes
CYP1A2 inhibitor		Yes	Yes	No
CYP2C19 inhibitor		No	No	No
CYP2C9 inhibitor		No	No	No

	Pecularity	7S4	SP600125	Pyrrolopyrimidine
	CYP2D6 inhibitor	No	No	No
	CYP3A4 inhibitor	No	No	No
	Log Kp (skin permeation)	-5.88 cm/s	-4.86 cm/s	-11.69 cm/s
Druglikeness	Lipinski	Yes; 0 violation	Yes; 0 violation	No; 2 violations: MW>500, NorO>10
	Ghose	Yes	Yes	No; 4 violations: MW>480, WLOGP<-0.4, MR>130, #atoms>70
	Veber	Yes	Yes	No; 1 violation: TPSA>140
	Egan	Yes	Yes	No; 1 violation: TPSA>131.6
	Muegge	Yes	Yes	No; 5 violations: MW>600, XLOGP3<-2, TPSA>150, #rings>7, H-acc>10
	Bioavailability Score	0.5	0.55	0.17

Molecular docking

In order to predict the JNK1 inhibitory activity of 7S4, molecular docking was performed. For the confirmation of the AutoDock Vina protocol, and its capability to predict the right poses, a well-studied JNK1 inhibitor, SP600125, and the native ligand in the structure of 3ELJ, the Pyrrolopyrimidine, were docked into the binding site, and then the binding affinities of 7S4, SP600125 and the Pyrrolopyrimidine were compared. According to the molecular docking results presented in Table 7, the binding affinities of 7S4, SP600125 and the Pyrrolopyrimidine to the JNK1 were -7.2, -9.7 and -6.4 kcal/mole, respectively. Therefore, it was concluded that 7S4 has higher JNK1 binding affinity than the Pyrrolopyrimidine but lesser than SP600125.

A comparative molecular visualization analysis of the 3D structure of JNK1 in complex with 7S4, SP600125 and the Pyrrolopyrimidine that were docked by AutoDock Vina was performed and the results were presented in Figure 8. N-terminal and C-terminal atoms of JNK1 were represented as spheres colored by blue and red, respectively. In addition, polypeptide chains were colored by the secondary structure. It was observed from Figure 8 that ASN-114 formed two different hydrogen bonds which are in lengths of 3.1 Å and 3.2 Å with 7S4. MET-111 formed a hydrogen bond which is in the length of 3.3 Å with SP600125. On the other hand, MET-111, GLU-109, MET-111, MET-111, ASN-114, SER-155 and ASN-156 residues formed six different hydrogen bonds which are in lengths of 3.3 Å, 2.9 Å, 3.0 Å, 3.0 Å, 3.2 Å, 3.2 Å, 3.0 Å with the Pyrrolopyrimidine. By relying on these findings, it was suggested that 7S4 targets JNK1, likewise SP600125 and the Pyrrolopyrimidine. In addition, since 7S4 is bound to the hydrophobic pocket of the ATP-binding site of JNK1 like SP600125 [36], it was suggested that 7S4 is a putative ATP-competitive inhibitor of JNK1.

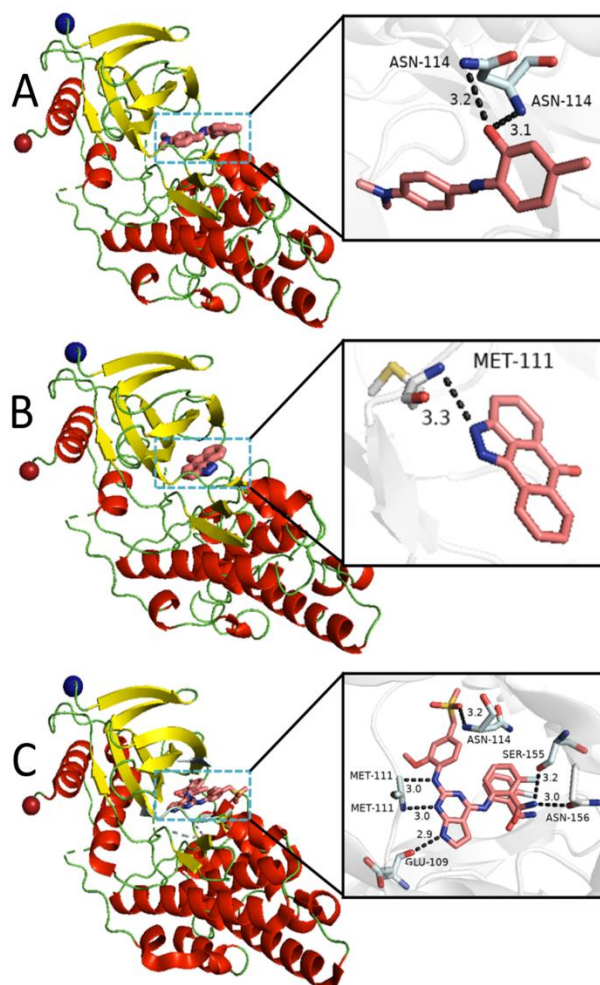


Figure 8: 3D structure of the JNK1 in complex with 7S4 (A), SP600125 (B) and the Pyrrolopyrimidine (C). Analysis of hydrogen bonds formed 7S4, SP600125 and the Pyrrolopyrimidine with JNK1.

Table 7. JNK1 docking of 7S4, SP600125 and the Pyrrolopyrimidine.

Protein	PDB Code	Ligand	ΔG (kcal/mole)	Interacting Residues	Distance (Å)
Crystal structure of JNK1	3ELJ	7S4	-7.2	ASN-114	3.1
				ASN-114	3.2
		SP600125	-9.7	MET-111	3.3
		Pyrrolopyrimidine	-6.4	GLU-109	2.9
				MET-111	3.0
				MET-111	3.0
ASN-114	3.2				
SER-155	3.2				
ASN-156	3.0				

4. Discussion and Conclusion

The compound 2-((4-(dimethylamino)benzylidene)amino)-5-methylphenol (7S4) was synthesized and the accuracy of the structure was proved by spectroscopic techniques (Supplementary materials1). In order to determine the most stable structure in the theoretical calculation, first of all, the stable structures of the possible trans and cis structures of the compound were examined. It was determined that the stable trans structure was 7S4_M7_7_E and the stable cis structure was 7S4_M27_27. Since the trans structure is the more stable structure between these two structures, all calculations were made with this stable trans structure. In addition, the possible tautomer form of the most stable trans structure (7S4_M7_7_K) was drawn. The possible stability of the enol (7S4_M7_7_E) and keto (7S4_M7_7_K)

forms of the stable trans structure was also investigated (Supplementary materials2, Supplementary materials3, Supplementary materials4 and Supplementary materials5).

From the calculations, it was determined that the most stable structure was 31_7S4_M7_7_E_scan15O_freq and all calculations were made with this structure. According to the calculation results, it was determined that the enol tautomer form was quite stable and the K_T balance was approximately 30-33 kcal/mole for all solvents. According to this result, it was concluded that the compound did not show keto tautomer and would only be in enol form (Table 2). All experimental and theoretical calculations will be performed on the enol structure of the compound only in this geometry. The compound has strong intramolecular H-bond (2.033 Å) between H16-N8 atoms (Figure 4). The presence of strong intramolecular H-bond means that this compound is highly stable in this geometry. Experimental and theoretical studies will be carried out on this geometry. From the dipole moment calculations, the dipole of the compound was determined to be quite high (in vacuum: 5.945, in other solvents 7.399-7.888) (Table 3). According to the dipole moment values, it is understood that the compound is a polar compound and will dissolve in polar and polar protic solvents. In experimental studies, it can be concluded that the best results will be in polar and polar protic medium. From NBO calculations, it was calculated that the most electron-rich atoms in the compound were O15 (Natural charge: -0.681), N8: (Natural charge: -0.514 and N18: (Natural charge: -0.477) (Table 4). These centers are active centers in electrophilic attacks. In addition, these centers play a role as active centers in chemical reactions, solvent-solute interactions, and biological systems. It was observed that the weakest center of the electron was the H16 atom (Natural charge: 0.489) (Table 4). The H16 atom is the most sensitive atom to the nucleophile. H16 is acidic hydrogen (PM6 method $pK_a=8.582$ by the MOPAC2016 package program) and reacts in a basic medium. It is concluded that the H16 atom will play a role as an active center in chemical reactions, nucleophilic attacks, basic reactions and biological systems. In addition, HOMO (-8.321 eV) and LUMO (-5.955 eV) energies were observed to be low (Figure 5). In addition, the E_{GAP} value is as low as 2.366 eV; It means that the compound is reactive in chemical reactions, is a colored compound and has a semiconductor feature. From the molecular electrostatic potential energy map, it was determined that the ring containing the OH group was the most electron-dense ring, the electron density gradually decreased towards the other ring, and the least electron density was on the $N(CH_3)_2$ group. In this compound, the red regions with high electron density are active centers against electrophiles, polar and polar protic solvents in solvent-solute interactions, and biological systems. Blue regions with low electron density are active centers against nucleophiles, and against polar and polar protic solvents in solvent-solute interactions and biological systems (Figure 6). From the solvent accessible surface area, polar and polar protic solvents are activated with blue and red colored atoms, and apolar solvents with gray colored atoms in chemical reactions and biological systems (Figure 7).

There are considerable efforts to design efficient drugs for the treatment of cancer. On the other hand, the burden of cancer incidence and mortality are rapidly growing across the world. The treatments generally fail with the effect of chemoresistance. Therefore, it is necessary to find novel cytotoxic chemicals that could be effective for the reversal of chemoresistance. In this study, 7S4 is suggested as a putative chemoresistance relieving agent with its affinity to JNK1, pharmacokinetic characteristics, and cytotoxic effects. The idea that 7S4 has an affinity to JNK1 relies on the observations from molecular docking analysis. In this experiment, the affinity of a widely used JNK1 inhibitor, SP600125, and a native ligand of JNK1, the Pyrrolopyrimidine, was compared with 7S4. It was observed that 7S4 has a better affinity than the native ligand but weaker affinity than the canonical JNK1 inhibitor. Thus, 7S4 could be used to develop an ATP-competitive inhibitor of JNK1. The pharmacokinetic characteristics, druglikeness and solubility of 7S4 are also promising to develop a therapeutic agent. Therefore, further experiments that aim to improve the therapeutic benefits of 7S4 could be promising for better therapy of cancer.

Acknowledgment

Authors are also grateful to Prof. Dr. Hülya Sivas, Ayşe Aydoğdu Erdönmez and Dila Ercengiz for their valuable contributions and suggestions.

The authors are thankful to the Anadolu University Scientific Research Projects (Project No. 1509F633 and 20ADP182) for financial support. The authors also grateful to Anadolu University Scientific Research commission for supporting Gaussian 09 (Project No:1102F027) and Gauss View 5.0 (Project

No: 1304F064) programs with the projects. We would like to thank to Anadolu University for providing the opportunity to use the CS ChemBioDraw Ultra 16.0.1.4 for Microsoft Windows program.

Declaration of Ethical Code

In this study, we undertake that all the rules required to be followed within the scope of the "Higher Education Institutions Scientific Research and Publication Ethics Directive" are complied with, and that none of the actions stated under the heading "Actions Against Scientific Research and Publication Ethics" are not carried out.

References

- [1] Sung, H., Ferlay, J., Siegel, R. L., Laversanne, M., Soerjomataram, I., Jemal, A., Bray, F. 2021. Global Cancer Statistics 2020: GLOBOCAN Estimates of Incidence and Mortality Worldwide for 36 Cancers in 185 Countries. *CA. Cancer J. Clin.*, 71 (3), 209–249. <https://doi.org/https://doi.org/10.3322/caac.21660>.
- [2] Zeytinoglu, H., Incesu, Z., Baser, K. H. C. 2003. Inhibition of DNA Synthesis by Carvacrol in Mouse Myoblast Cells Bearing a Human N-RAS Oncogene. *Phytomedicine*, 10 (4), 292–299. <https://doi.org/https://doi.org/10.1078/094471103322004785>.
- [3] Demiroglu-Zergeroglu, A., Ergene, E., Ayvali, N., Kuete, V., Sivas, H. 2016. Quercetin and Cisplatin Combined Treatment Altered Cell Cycle and Mitogen Activated Protein Kinase Expressions in Malignant Mesotelioma Cells. *BMC Complement. Altern. Med.* 16 (1), 281. <https://doi.org/10.1186/s12906-016-1267-x>.
- [4] Uysal, U. D., Ercengiz, D., Karaosmanoğlu, O., Berber, B., Sivas, H., Berber, H. 2021. Theoretical and Experimental Electronic Transition Behaviour Study of 2-((4-(Dimethylamino)Benzylidene)Amino)-4-Methylphenol and Its Cytotoxicity. *J. Mol. Struct.*, 1227, 129370. <https://doi.org/https://doi.org/10.1016/j.molstruc.2020.129370>.
- [5] Borges, A. A., de Souza, M. P., da Fonseca, A. C. C., Wermelinger, G. F., Ribeiro, R. C. B., Amaral, A. A. P., de Carvalho, C. J. C., Abreu, L. S., de Queiroz, L. N., de Almeida, E. C. P., Rabelo, V. W., Abreu, P. A., Pontes, B., Ferreira, V. F., da Silva, F. de C., Forezi, L. da S. M., Robbs, B. K. 2022. Chemoselective Synthesis of Mannich Adducts from 1,4-Naphthoquinones and Profile as Autophagic Inducers in Oral Squamous Cell Carcinoma. *Molecules*, 28 (1), 309. <https://doi.org/10.3390/molecules28010309>.
- [6] Di Micco, S., Di Sarno, V., Rossi, M., Vestuto, V., Konno, T., Novi, S., Tecce, M. F., Napolitano, V., Ciaglia, T., Vitale, A., Gomez-Monterrey, I. M., Bifulco, G., Bertamino, A., Ostacolo, C., Blasi, P., Fasano, A., Campiglia, P., Musella, S. 2022. In Silico Identification and In Vitro Evaluation of New ABCG2 Transporter Inhibitors as Potential Anticancer Agents. *Int. J. Mol. Sci.*, 24 (1), 725. <https://doi.org/10.3390/ijms24010725>.
- [7] Liu, Z., Zou, H., Dang, Q., Xu, H., Liu, L., Zhang, Y., Lv, J., Li, H., Zhou, Z., Han, X. 2022. Biological and Pharmacological Roles of M6A Modifications in Cancer Drug Resistance. *Mol. Cancer*, 21 (1), 220. <https://doi.org/10.1186/s12943-022-01680-z>.
- [8] Bonventre, J. V. 2003. Molecular Response to Cytotoxic Injury: Role of Inflammation, MAP Kinases, and Endoplasmic Reticulum Stress Response. *Semin. Nephrol.*, 23 (5), 439–448. [https://doi.org/https://doi.org/10.1016/S0270-9295\(03\)00115-3](https://doi.org/https://doi.org/10.1016/S0270-9295(03)00115-3).
- [9] Lipner, M. B., Peng, X. L., Jin, C., Xu, Y., Gao, Y., East, M. P., Rashid, N. U., Moffitt, R. A., Herrera Loeza, S. G., Morrison, A. B., Goltz, B. T., Vaziri, C., Graves, L. M., Johnson, G. L., Yeh, J. J. 2020. Irreversible JNK1-JUN Inhibition by JNK-IN-8 Sensitizes Pancreatic Cancer to 5-FU/FOLFOX Chemotherapy. *JCI Insight*, 5 (8). <https://doi.org/10.1172/jci.insight.129905>.
- [10] Li, F., Meng, L., Zhou, J., Xing, H., Wang, S., Xu, G., Zhu, H., Wang, B., Chen, G., Lu, Y.-P., Ma, D. 2005. Reversing Chemoresistance in Cisplatin-Resistant Human Ovarian Cancer Cells: A Role of c-Jun NH2-Terminal Kinase 1. *Biochem. Biophys. Res. Commun.*, 335 (4), 1070–1077. <https://doi.org/https://doi.org/10.1016/j.bbrc.2005.07.169>.
- [11] Liu, X.-Y., Liu, S.-P., Jiang, J., Zhang, X., Zhang, T. 2016. Inhibition of the JNK Signaling Pathway Increases Sensitivity of Hepatocellular Carcinoma Cells to Cisplatin by Down-Regulating Expression of P-Glycoprotein. *Eur. Rev. Med. Pharmacol. Sci.*, 20 (6), 1098–1108.
- [12] Shinoda, C., Maruyama, M., Fujishita, T., Dohkan, J., Oda, H., Shinoda, K., Yamada, T., Miyabayashi, K., Hayashi, R., Kawagishi, Y., Fujita, T., Matsui, S., Sugiyama, E., Muraguchi, A., Kobayashi, M. 2005. Doxorubicin Induces Expression of Multidrug Resistance-Associated Protein 1 in Human Small Cell Lung

- Cancer Cell Lines by the c-Jun N-Terminal Kinase Pathway. *Int. J. Cancer*, 117 (1), 21–31. <https://doi.org/https://doi.org/10.1002/ijc.21094>.
- [13] Kim, J.-H., Lee, S. C., Ro, J., Kang, H. S., Kim, H. S., Yoon, S. 2010. Jnk Signaling Pathway-Mediated Regulation of Stat3 Activation Is Linked to the Development of Doxorubicin Resistance in Cancer Cell Lines. *Biochem. Pharmacol.*, 79 (3), 373–380. <https://doi.org/https://doi.org/10.1016/j.bcp.2009.09.008>.
- [14] Kim, J.-H., Kim, T. H., Kang, H. S., Ro, J., Kim, H. S., Yoon, S. 2009. SP600125, an Inhibitor of Jnk Pathway, Reduces Viability of Relatively Resistant Cancer Cells to Doxorubicin. *Biochem. Biophys. Res. Commun.*, 387 (3), 450–455. <https://doi.org/https://doi.org/10.1016/j.bbrc.2009.07.036>.
- [15] Liu, Y., Zhang, X., Wang, J., Yang, J., Tan, W. 2015. JNK Is Required for Maintaining the Tumor-Initiating Cell-like Properties of Acquired Chemoresistant Human Cancer Cells. *Acta Pharmacol. Sin.*, 36 (9), 1099–1106. <https://doi.org/10.1038/aps.2015.58>.
- [16] Zhu, M. M., Tong, J. L., Xu, Q., Nie, F., Xu, X. T., Xiao, S. D., Ran, Z. H. 2012. Increased JNK1 Signaling Pathway Is Responsible for ABCG2-Mediated Multidrug Resistance in Human Colon Cancer. *PLoS One*, 7 (8), e41763.
- [17] Vasilevska, I. A., Selvakumaran, M., Roberts, D., O'Dwyer, P. J. 2016. JNK1 Inhibition Attenuates Hypoxia-Induced Autophagy and Sensitizes to Chemotherapy. *Mol. Cancer Res.*, 14 (8), 753 LP – 763. <https://doi.org/10.1158/1541-7786.MCR-16-0035>.
- [18] Wu, Q., Wu, W., Jacevic, V., Franca, T. C. C., Wang, X., Kuca, K. 2020. Selective Inhibitors for JNK Signalling: A Potential Targeted Therapy in Cancer. *J. Enzyme Inhib. Med. Chem.*, 35 (1), 574–583. <https://doi.org/10.1080/14756366.2020.1720013>.
- [19] Roskoski, R. 2019. Properties of FDA-Approved Small Molecule Protein Kinase Inhibitors. *Pharmacol. Res.*, 144, 19–50. <https://doi.org/https://doi.org/10.1016/j.phrs.2019.03.006>.
- [20] Berhanu, A. L., Gaurav, Mohiuddin, I., Malik, A. K., Aulakh, J. S., Kumar, V., Kim, K.-H. 2019. A Review of the Applications of Schiff Bases as Optical Chemical Sensors. *TrAC Trends Anal. Chem.*, 116, 74–91. <https://doi.org/https://doi.org/10.1016/j.trac.2019.04.025>.
- [21] Yu, X., Wang, K., Cao, D., Liu, Z., Guan, R., Wu, Q., Xu, Y., Sun, Y., Zhao, X. 2017. A Diethylamino Pyridine Formyl Schiff Base as Selective Recognition Chemosensor for Biological Thiols. *Sensors Actuators B Chem.*, 250, 132–138. <https://doi.org/https://doi.org/10.1016/j.snb.2017.04.147>.
- [22] Kajal, A., Bala, S., Kamboj, S., Sharma, N., Saini, V. 2013. Schiff Bases: A Versatile Pharmacophore. *J. Catal.*, 2013, 893512. <https://doi.org/10.1155/2013/893512>.
- [23] Sıdır, İ., Sıdır, Y. G., Berber, H., Demiray, F. 2019. Electronic Structure and Optical Properties of Schiff Base Hydrazone Derivatives by Solution Technique for Optoelectronic Devices: Synthesis, Experiment and Quantum Chemical Investigation. *J. Mol. Struct.*, 1176, 31–46. <https://doi.org/https://doi.org/10.1016/j.molstruc.2018.08.067>.
- [24] Sıdır, Y. G., Aslan, C., Berber, H., Sıdır, İ. 2019. The Electronic Structure, Solvatochromism, and Electric Dipole Moments of New Schiff Base Derivatives Using Absorbance and Fluorescence Spectra. *Struct. Chem.*, 30 (3), 835–851. <https://doi.org/10.1007/s11224-018-1228-8>.
- [25] Sıdır, Y. G., Pirbudak, G., Berber, H., Sıdır, İ. 2017. Study on the Electronic and Photophysical Properties of the Substitute-((2-Phenoxybenzylidene)Amino)Phenol Derivatives: Synthesis, Solvatochromism, Electric Dipole Moments and DFT Calculations. *J. Mol. Liq.*, 242, 1096–1110. <https://doi.org/https://doi.org/10.1016/j.molliq.2017.07.070>.
- [26] Gowda, A., Roy, A., Kumar, S. 2017. Synthesis and Mesomorphic Properties of Novel Schiff Base Liquid Crystalline EDOT Derivatives. *J. Mol. Liq.*, 225, 840–847. <https://doi.org/https://doi.org/10.1016/j.molliq.2016.11.010>.
- [27] Kausar, N., Muratza, S., Raza, M. A., Rafique, H., Arshad, M. N., Altaf, A. A., Asiri, A. M., Shafqat, S. S., Shafqat, S. R. 2019. Sulfonamide Hybrid Schiff Bases of Anthranilic Acid: Synthesis, Characterization and Their Biological Potential. *J. Mol. Struct.*, 1185, 8–20. <https://doi.org/https://doi.org/10.1016/j.molstruc.2019.02.056>.
- [28] Ünver, H., Boyacıoğlu, B., Zeyrek, C. T., Yıldız, M., Demir, N., Yıldırım, N., Karaosmanoğlu, O., Sivas, H., Elmali, A. 2016. Synthesis, Spectral and Quantum Chemical Studies and Use of (E)-3-[(3,5-Bis(Trifluoromethyl)Phenylimino)Methyl]Benzene-1,2-Diol and Its Ni(II) and Cu(II) Complexes as an Anion

- Sensor, DNA Binding, DNA Cleavage, Anti-Microbial, Anti-Mutagenic and Anti-Canc. *J. Mol. Struct.*, 1125. <https://doi.org/10.1016/j.molstruc.2016.06.058>.
- [29] Judith Percino, M., Cerón, M., Castro, M. E., Ramírez, R., Soriano, G., Chapela, V. M. 2015. (E)-2-[(2-Hydroxybenzylidene)Amino]Phenylarsonic Acid Schiff Base: Synthesis, Characterization and Theoretical Studies. *J. Mol. Struct.*, 1081, 193–200. <https://doi.org/10.1016/j.molstruc.2014.10.030>.
- [30] Alpaslan, G., Boyacioglu, B., Demir, N., Tümer, Y., Yapar, G., Yıldırım, N., Yıldız, M., Ünver, H. 2019. Synthesis, Characterization, Biological Activity and Theoretical Studies of a 2-Amino-6-Methoxybenzothiazole-Based Fluorescent Schiff Base. *J. Mol. Struct.*, 1180, 170–178. <https://doi.org/10.1016/j.molstruc.2018.11.065>.
- [31] Cunha Almeida, T., Gonzaga Ribeiro, L. H., Ferreira dos Santos, L. B., da Silva, C. M., Tupinambá Branquinho, R., de Lana, M., Ramos Gadelha, F., de Fátima, Â. 2018. Synthesis, in Vitro and in Vivo Anti-Trypanosoma Cruzi and Toxicological Activities of Nitroaromatic Schiff Bases. *Biomed. Pharmacother.*, 108, 1703–1711. <https://doi.org/10.1016/j.biopha.2018.09.176>.
- [32] Saadaoui, I., Krichen, F., Ben Salah, B., Ben Mansour, R., Miled, N., Bougatef, A., Kossentini, M. 2019. Design, Synthesis and Biological Evaluation of Schiff Bases of 4-Amino-1,2,4-Triazole Derivatives as Potent Angiotensin Converting Enzyme Inhibitors and Antioxidant Activities. *J. Mol. Struct.*, 1180, 344–354. <https://doi.org/10.1016/j.molstruc.2018.12.008>.
- [33] Zaltariov, M.-F., Avadanei, M., Balan, M., Peptanariu, D., Vornicu, N., Shova, S. 2019. Synthesis, Structural Characterization and Biological Studies of New Schiff Bases Containing Trimethylsilyl Groups. *J. Mol. Struct.*, 1175, 624–631. <https://doi.org/10.1016/j.molstruc.2018.08.019>.
- [34] Al-Shemary, R. K. R., Al-khazraji, A. M. A., Niseaf, A. N. 2016. Preparation, Spectroscopic Study of Schiff Base Ligand Complexes with Some Metal Ions and Evaluation of Antibacterial Activity. *Pharma Innov. J.*, 5, 81–86.
- [35] Heo, Y.-S., Kim, S.-K., Seo, C. II, Kim, Y. K., Sung, B.-J., Lee, H. S., Lee, J. II, Park, S.-Y., Kim, J. H., Hwang, K. Y., Hyun, Y.-L., Jeon, Y. H., Ro, S., Cho, J. M., Lee, T. G., Yang, C.-H. 2004. Structural Basis for the Selective Inhibition of JNK1 by the Scaffolding Protein JIP1 and SP600125. *EMBO J.*, 23 (11), 2185–2195. <https://doi.org/10.1038/sj.emboj.7600212>.
- [36] Chamberlain, S. D., Redman, A. M., Wilson, J. W., Deanda, F., Shotwell, J. B., Gerding, R., Lei, H., Yang, B., Stevens, K. L., Hassell, A. M., Shewchuk, L. M., Leesnitzer, M. A., Smith, J. L., Sabbatini, P., Atkins, C., Groy, A., Rowand, J. L., Kumar, R., Mook, R. A., Moorthy, G., Patnaik, S. 2009. Optimization of 4,6-Bis-Anilino-1H-Pyrrolo[2,3-d]Pyrimidine IGF-1R Tyrosine Kinase Inhibitors towards JNK Selectivity. *Bioorg. Med. Chem. Lett.*, 19 (2), 360–364. <https://doi.org/10.1016/j.bmcl.2008.11.077>.
- [37] Bennett, B. L., Sasaki, D. T., Murray, B. W., O’Leary, E. C., Sakata, S. T., Xu, W., Leisten, J. C., Motiwala, A., Pierce, S., Satoh, Y., Bhagwat, S. S., Manning, A. M., Anderson, D. W. 2001. SP600125, an Anthrapyrazolone Inhibitor of Jun N-Terminal Kinase. *Proc. Natl. Acad. Sci.*, 98 (24), 13681–13686. <https://doi.org/10.1073/pnas.251194298>.
- [38] Li, P., Zhao, Q.-L., Rehman, M., Jawaid, P., Cui, Z.-G., Ahmed, K., Kondo, T., Saitoh, J.-I., Noguchi, K. 2023. Isofraxidin Enhances Hyperthermia-induced Apoptosis via Redox Modification in Acute Monocytic Leukemia U937 Cells. *Mol. Med. Rep.*, 27 (2), 41. <https://doi.org/10.3892/mmr.2023.12928>.
- [39] Yuan, M.-K., Kao, J.-W., Wu, W.-T., Chen, C.-R., Chang, C.-I., Wu, Y.-J. 2022. Investigation of Cell Cytotoxic Activity and Molecular Mechanism of 5 β ,19-Epoxycucurbita-6,23(E)-Diene-3 β ,19(R),25-Triol Isolated from *Momordica Charantia* on Hepatoma Cells. *Pharm. Biol.*, 60 (1), 1214–1223. <https://doi.org/10.1080/13880209.2022.2077766>.
- [40] Frisch, M. J., Trucks, G. W., Schlegel, H. B., Scuseria, G. E., Robb, M. A., Cheeseman, J. R., Scalmani, G., Barone, V., Mennucci, B., Petersson, G. A., Nakatsuji, H., Caricato, M., Li, X., Hratchian, H. P., Izmaylov, A. F., Bloino, J., Zheng, G., Sonnenberg, J. L., Hada, M., Ehara, M., Toyota, K., Fukuda, R., Hasegawa, J., Ishida, M., Nakajima, T., Honda, Y., Kitao, O., Nakai, H., Vreven, T., Montgomery, J. A., Peralta, J. E., Ogliaro, F., Bearpark, M., Heyd, J. J., Brothers, E., Kudin, K. N., Staroverov, V. N., Kobayashi, R., Normand, J., Raghavachari, K., Rendell, A., Burant, J. C., Iyengar, S. S., Tomasi, J., Cossi, M., Rega, N., Millam, J. M., Klene, M., Knox, J. E., Cross, J. B., Bakken, V., Adamo, C., Jaramillo, J., Gomperts, R., Stratmann, R. E., Yazyev, O., Austin, A. J., Cammi, R., Pomelli, C., Ochterski, J. W., Martin, R. L., Morokuma, K., Zakrzewski, V. G., Voth, G. A., Salvador, P., Dannenberg, J. J., Dapprich, S., Daniels, A. D., Farkas, Ö., Foresman, J. B., Ortiz, J. V., Cioslowski, J., Fox, D. J. Gaussian 09 Revision A.2. 2009.
- [41] Dennington, R., Keith, T., Millam, J. GaussView. Semichem Inc.: Shawnee Mission, KS 2009.

- [42] CS ChemBioDraw Ultra 16.0.1.4 for Microsoft Windows.
- [43] MarvinSketch 19.27.0.
- [44] Kuete, V., Ngnintedo, D., Fotso, G. W., Karaosmanoğlu, O., Ngadjui, B. T., Keumedjio, F., Yeboah, S. O., Andrae-Marobela, K., Sivas, H. 2018. Cytotoxicity of Seputhecarpan D, Thonningiol and 12 Other Phytochemicals from African Flora towards Human Carcinoma Cells. *BMC Complement. Altern. Med.*, 18 (1), 36. <https://doi.org/10.1186/s12906-018-2109-9>.
- [45] Daina, A., Michielin, O., Zoete, V. 2017. SwissADME: A Free Web Tool to Evaluate Pharmacokinetics, Drug-Likeness and Medicinal Chemistry Friendliness of Small Molecules. *Sci. Rep.*, 7 (1), 42717. <https://doi.org/10.1038/srep42717>.
- [46] Morris, G. M., Huey, R., Lindstrom, W., Sanner, M. F., Belew, R. K., Goodsell, D. S., Olson, A. J. 2009. AutoDock4 and AutoDockTools4: Automated Docking with Selective Receptor Flexibility. *J. Comput. Chem.*, 30 (16), 2785–2791. <https://doi.org/10.1002/jcc.21256>.
- [47] Trott, O., Olson, A. J. 2010. AutoDock Vina: Improving the Speed and Accuracy of Docking with a New Scoring Function, Efficient Optimization, and Multithreading. *J. Comput. Chem.*, 31 (2), 455–461. <https://doi.org/10.1002/jcc.21334>.
- [48] L DeLano, W. 2002. Pymol: An Open-Source Molecular Graphics Tool. *{CCP4} Newsl. Protein Crystallogr.*, 40, 82–92.